Radioresistant cells initiate lymphocyte-dependent lung inflammation and IFNγ-dependent mortality in STING gain-of-function mice

Kevin MingJie Gao[a,b] (ID), Mona Motwani[a], Thomas Tedder[c,d], Ann Marshak-Rothstein[a,b,1,2], and Katherine A. Fitzgerald[a,1,2]

Pediatric patients with constitutively active mutations in the cytosolic double-stranded-DNA-sensing adaptor STING develop an autoinflammatory syndrome known as STING-associated vasculopathy with onset in infancy (SAVI). SAVI patients have elevated interferon-stimulated gene expression and suffer from interstitial lung disease (ILD) with lymphocyte predominate bronchus-associated lymphoid tissue (BALT). Mice harboring SAVI mutations (STING V154M [VM]) that recapitulate human disease also develop lymphocyte-rich BALT. Ablation of either T or B lymphocytes prolongs the survival of SAVI mice, but lung immune aggregates persist, indicating that T cells and B cells can independently be recruited as BALT. VM T cells produced IFNγ, and IFNγR deficiency prolonged the survival of SAVI mice; however, T-cell-dependent recruitment of infiltrating myeloid cells to the lung was IFNγ independent. Lethally irradiated VM recipients fully reconstituted with wild type bone-marrow-derived cells still developed ILD, pointing to a critical role for VM-expressing radioresistant parenchymal and/or stromal cells in the recruitment and activation of pathogenic lymphocytes. We identified lung endothelial cells as radioresistant cells that express STING. Transcriptional analysis of VM endothelial cells revealed up-regulation of chemokines, proinflammatory cytokines, and genes associated with antigen presentation. Together, our data show that VM-expressing radioresistant cells play a key role in the initiation of lung disease in VM mice and provide insights for the treatment of SAVI patients, with implications for ILD associated with other connective tissue disorders.

SAVI | STING | interferon gamma | interstitial lung disease | endothelial cells

The lung is a critical mucosal barrier, which is continuously challenged by environmental stressors such as infection and pollution, that can precipitate inflammation and compromise respiratory function. In genetically susceptible individuals, chronic inflammation and lung damage can result in a heterogeneous category of diseases known as interstitial lung disease (ILD). The processes that elicit ILD are poorly understood; indeed, ILD is diagnosed in 70% of patients without a clear identification of etiology. For those 30% of patients diagnosed with ILD of an attributable cause, over half are thought to develop ILD as a presentation of rheumatic disease and are commonly referred to as connective tissue disorder interstitial lung disease (CTD-ILD) (1–4).

The cGAS-STING double-stranded-DNA-sensing pathway serves as a frontline of antiviral, antibacterial, and antitumor immunity, in part through the production of type 1 interferons (IFN). Gain-of-function (GOF) mutations in the dimerization domain of STING result in constitutive ligand independent activation and precipitate a severe autoinflammatory syndrome in pediatric patients known as STING-associated vasculopathy with onset in infancy (SAVI). Over 80 SAVI patients have now been identified. Surveys of these patients show a diverse presentation of clinical findings including severe skin lesions, arthropathy, glomerulonephritis, colitis, and basal ganglia calcifications. Importantly, nearly all SAVI patients develop severe ILD and commonly succumb to respiratory failure early in life (5, 6).

Human SAVI ILD is characterized by abnormal pulmonary function, prominent lung computed tomography (CT) findings, elevated neutrophil and lymphocyte counts in bronchoalveolar lavage fluid, and histopathologic findings of lymphocytic infiltrates. While other manifestations of SAVI disease respond to immune suppression, especially by treatment with JAK-STAT inhibitors, SAVI ILD is highly recalcitrant to immunosuppressive therapies (6–8). It remains unknown why SAVI disease presents most consistently as a lung disease and how STING initiates inflammation in the lung. A better understanding of how STING promotes lung inflammation is not only relevant for the treatment of SAVI patients but also may reveal when, where, and how this nucleic-acid-sensing pathway contributes to pulmonary pathophysiology in other contexts.

Significance

cGAS-STING is a DNA-sensing pathway that protects against pathogens and cancer, but activating mutations in STING lead to an autoinflammatory disease known as STING-associated vasculopathy with onset in infancy (SAVI) that predominately features interstitial lung disease (ILD). In this study, a SAVI mouse model was used to demonstrate that IFNγ and T cells promote lung inflammation and reduce the lifespan of SAVI mice. Moreover, we discovered that SAVI ILD was initiated by radioresistant nonimmune cells and reveal that SAVI endothelia are activated and may contribute to this initiation. These data not only identify key mechanisms of SAVI disease but also elucidate the underlying biology of STING in the lung that likely extends to other settings of pulmonary inflammation.

Mechanistic insights into human disease can be gleaned from animal models. We and others have leveraged CRISPR-Cas9 to engineer gene-targeted mice that express the two most common SAVI alleles seen in human patients, namely, STING V154M (seen in about 60% of patients; VM), and STING N153S (seen in about 25% of patients; NS) (6). These mutations result in severe lung pathology associated with prominent immune aggregates and reduced survival, with VM mice expressing the more robust phenotype (9–11). These SAVI mouse models have helped elucidate mechanistic underpinnings of lung pathology. For example, while SAVI patients and mice have elevated titers of type I IFN, increased expression of interferon-stimulated genes (ISGs) and SAVI is commonly referred to as a type 1 interferonopathy, deficiency of either IRF3 or the IFNαR receptor fails to attenuate lung disease or improve survival in SAVI mice (11, 12). Instead, studies using the NS model of SAVI have unveiled a central role for T cells but not B cells in SAVI lung pathology (12). Moreover, crossing NS mice to the OT-I TCR transgenic line to restrict the T cell compartment to CD8 T cells specific for the irrelevant antigen OVA also prevents lung pathology (13). Additionally, radiation chimera experiments using SAVI mice have concluded that features of myeloid expansion and lymphopenia are due to cell-intrinsic STING GOF, whereas wild-type (WT) mice reconstituted with bone marrow (BM) from SAVI donors present with minimal lung disease (11, 12). Interestingly, previous studies indicated that chimeric NS mice reconstituted with WT BM still developed severe lung pathology; however, because donor and host cells were not allotypically distinct, the possibility of radioresistant immune cells reinitiating disease could not be ruled out (12).

In this study, we hypothesized that lymphocytes would be required for lung pathology in the VM SAVI mouse model but that stromal and/or parenchymal lung cells expressing the VM mutation would initiate their activation and recruitment. Tertiary lymphoid organs in the lung known as bronchus-associated lymphoid tissue (BALT) are commonly observed in CTD-ILD and are regarded as organizing centers of inflammation in tissues (14). We demonstrate that organized BALT comprised of both B and T cells accrue in the VM SAVI lung and that B and T cell deficiency both improve survival. However, lymphocytes per se do not need to express the VM mutation. Rather, VM-expressing radioresistant stromal and parenchymal cells appear to trigger BALT pathology. We identify endothelial cells as STING-expressing stromal cells that up-regulate immune function in the setting of STING GOF. Lastly, we provide evidence that SAVI lung T lymphocytes promote mortality through IFNγ production and that IFNγ also potentiates the antigen presentation function of lung endothelium by up-regulating MHCII.

Results

VM Mice Develop ILD with BALT. While it is known that SAVI mice spontaneously develop inflammatory histopathology, more in-depth studies to assess the inflammatory infiltrate within murine SAVI lung and its consequence on pulmonary function have been lacking. To better understand how the murine VM SAVI model compares to human SAVI disease, we performed a detailed assessment of pulmonary pathology in 4- to 5-mo-old VM mice.

Lung micro-CT scans showed that VM mice develop perilymphatic nodular opacities (Fig. 1A, Bottom), which were not apparent in WT control mice (Fig. 1A, Top). Lung histopathologic assessment of the same mice confirmed that these nodular
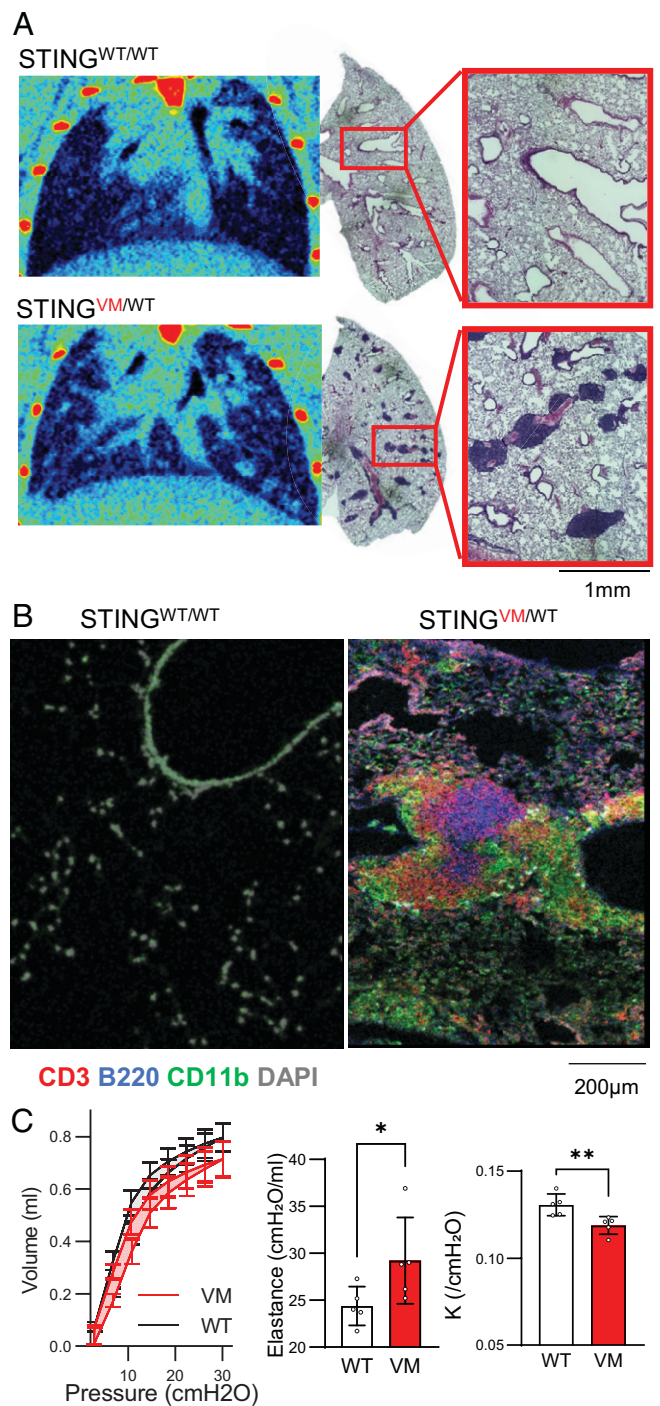

Fig. 1. VM mice develop ILD with BALT. (A) Four- to 5-mo-old littermate- and sex-matched WT and VM mice were assessed by micro-CT coronal cross-sections of lung field from representative WT and VM mice and H&E histology from the same individual mice. (B) IF imaging of 5-mo-old WT and VM lung stained for CD3 (red), B220 (blue), CD11b (green), and DAPI (gray). (C) Ventilography measurements from WT (n = 5) and VM (n = 5) mice showing pressure-volume loop, elastance, and K (curvature of the upper portion of pressure-volume loop deflation limb). Nonparametric Mann–Whitney U tests were used to determine statistical significance (*P < 0.05, **P < 0.01).

opacities corresponded to aggregates of immune cells that were primarily arranged around bronchovascular bundles. Examination of these immune aggregates by immunofluorescent (IF) microscopy found them to be organized and comprised of a central B220^{+} B cell zone and a surrounding CD3^{+} T cell zone as well as peripheral CD11b^{+} myeloid cells (Fig. 1B),

consistent with identification as BALT. Additionally, when mice were euthanized at 4 to 5 mo of age, VM mice frequently presented with a milky white exudative pleural effusion rich for immune cells, particularly neutrophils (*SI Appendix*, Fig. S1*A*). Sampling of the bronchoalveolar space by lavage also demonstrated an enrichment of neutrophils both by composition and absolute number in VM mice, while total numbers of T cells and SiglecF$^+$CD11c$^+$ alveolar macrophages in this BALF were similar in WT and VM mice (*SI Appendix*, Fig. S1*B*).

These inflammatory changes were associated with altered pulmonary function. Quantification of respiratory mechanics demonstrated that VM mice had a deflated pressure–volume loop curvature along with higher elastance, consistent with a restrictive pattern of pulmonary function (Fig. 1*C*). Together, these findings support a presentation of follicular bronchiolitis (FB) or lymphocytic interstitial pneumonitis (LIP), which are both considered forms of ILD (15).

B and T Cells Independently Contribute to BALT Formation and Reduce Survival of VM Mice. The abundant myeloid infiltrates in VM mice seen by immunofluorescence microscopy were consistent with previous studies demonstrating that VM mice exhibit enhanced myelopoiesis (11). However, the presence of lymphocyte-rich BALT in the lung contrasted with previously documented peripheral lymphopenia of both B and T cells. Thus, despite a paucity of splenic B and T cells, lymphocytes accumulated in the VM lung, and we hypothesized that the lymphocytes accumulating in the VM lung contributed to lung disease. Immune aggregate formation on whole-lung sections was quantified using a semiautomated pixel classification approach. This strategy demonstrated significant enrichment of these lesions in VM lung compared to WT (Fig. 2 *A* and *B*).

Next, to test the independent role of B and αβ T cells on VM disease, we crossed VM mice to mice with a μMT or TCRβ deficiency, respectively, and found BALT pathology persisted in both VM μMT knockout (KO) and VM TCRβ KO mice (Fig. 2*B*). However, a morphologic comparison of BALT between VM, VM TCRβ KO, and VM μMT KO mice suggested that B and T cells contribute to distinct aspects of BALT organization (Fig. 2*A*). While VM BALT are predominately large continuous aggregates that wrap around bronchovascular bundles, BALT in VM TCRβ KO feature smaller, separated, circular aggregates suggestive of B cell follicles; whereas BALT in VM μMT KO show numerous small, scattered lesions contiguous to bronchovascular bundles. Taken together, these observations suggest that while B and T cells can be independently recruited to the VM lung, both populations cooperate to form larger organized BALT structures (Fig. 2*A*).

Despite the persistence of BALT in both VM μMT KO and VM TCRβ KO mice, both circumstances extended the VM SAVI lifespan (Fig. 2*C*). A total of 25% of VM mice died by 74 d, in comparison to VM TCRβKO mice at 152 d and VM μMT KO mice at 109 d. Although the overall lifespan of VM μMT KO mice did not significantly differ from VM (*P* = 0.2073), depleting B cells in VM mice with CD20 monoclonal antibodies (mAbs) did confer a significant survival benefit compared to isotype-treated controls. VM mice treated with CD20 mAbs also showed persistent BALT pathology (Fig. 2 *D* and *E*). Together, these findings indicate that both B and αβ T cells contribute to VM SAVI mortality, although the survival benefit in VM TCRβ KO mice was more significant than that of VM μMT KO and CD20-mAb-treated VM mice (Fig. 2*D*).

VM SAVI T Cells Produce IFNγ, and IFNγR Contributes to VM SAVI Mortality. Given that αβ T cells are recruited to the VM lung and contribute to mortality, we sought to understand how these αβ T cells promote disease. To assess the cytokine-producing potential of VM T cells, we assayed the culture supernatants of purified CD4$^+$ splenic T cells stimulated with CD3 and CD28 mAbs. VM CD4$^+$ T cells secreted higher levels of IFNγ but lower levels of IL-4 and IL-17 compared to WT controls, pointing to a Th1-like phenotype (*SI Appendix*, Fig. S2*A*). Additionally, purified VM CD8$^+$ T cells also secreted higher levels of IFNγ and TNFα than WT controls, consistent with skewing toward a Tc1 state (*SI Appendix*, Fig. S2*A*). Moreover, splenic VM CD4 and CD8 T cells stimulated with CD3 and CD28 mAbs in the presence of brefeldin A were significantly enriched for IFNγ$^+$-producing cells compared to WT controls as shown by cytoplasmic staining (Fig. 3 *A* and *B*). VM splenic T cells treated with brefeldin-A in the absence of additional stimulation also showed enrichment for IFNγ-producing CD4$^+$ T cells (*SI Appendix*, Fig. S2*B*). When T cells isolated from the VM lung were treated with brefeldin A, both CD4$^+$ and CD8$^+$ αβ extravascular (EV) T cells showed a higher frequency of IFNγ$^+$ cells than WT control cells, although CD8 T cell IFNγ production did not reach statistical significance of $P < 0.05$ ($P = 0.1470$) (Fig. 3 *A* and *B*).

These data suggested that T cell production of IFNγ might be a mechanism through which VM T cells promote lung pathology and mortality. To test this hypothesis, VM mice were intercrossed with IFNγR-deficient mice to generate VM IFNγR KO mice. While VM IFNγR KO mice still developed BALT (Fig. 3 *C* and *D*), survival was significantly improved as in VM TCRβ KO mice, with 25% of VM IFNγR KO mice dying at 132 d in comparison to 74 d for VM mice and 156 d for VM TCRβ KO mice (Figs. 2*C* and 3*E*).

VM T Cells Promote Lung Lymphocyte Activation and Myeloid Recruitment. Despite improvements in survival, VM TCRβ KO and VM IFNγR KO mice persisted in the development of BALT, suggesting that qualitative changes in the lung-resident immune populations were playing a role in the severity of disease. To quantify the lung-resident immune cells of VM mice, we used flow cytometry and distinguished intravascular immune cells from EV immune cells by labeling circulating immune cells with an intravenously-injected fluorophore-conjugated CD45 antibody, sacrificing the mice 3 min later, and then enzymatically and mechanically dissociating the lungs to generate single-cell suspensions. Consistent with the IF microscopy showing BALT, VM lungs were significantly enriched for EV B and T lymphocytes as well as myeloid cells (Fig. 4*A*), whereas lungs from uninflamed WT, μMT KO, IFNγR KO, and TCRβ KO mice showed similarly low numbers of EV immune cells consistent with a lack of BALT pathology (*SI Appendix*, Fig. S3).

Because we had demonstrated that BALT persists in VM μMT and VM TCRβ KO mice, we predicted that B and T lymphocytes would accumulate in the lung independent of one another. Indeed, we saw by fluorescence-activated cell sorting that EV B cells persisted in VM TCRβ KO mice and that EV αβ T cells persisted in VM μMT KO mice (Fig. 4*A*). VM TCRβ-deficient mice retain TCRγδ T cells, and γδ T cells undergo compensatory expansion in the absence of αβ T cells in the lung (*SI Appendix*, Fig. S4*A*). To rule out the possibility that γδ T cells were involved in VM TCRαβ KO BALT pathology, we generated VM TCRβ KO TCRδ KO mice and found BALT pathology persisted with enrichment of EV B cells (*SI Appendix*, Fig. S4 *B* and *C*), indicating that neither αβ nor γδ T cells are required for B recruitment and maintenance.
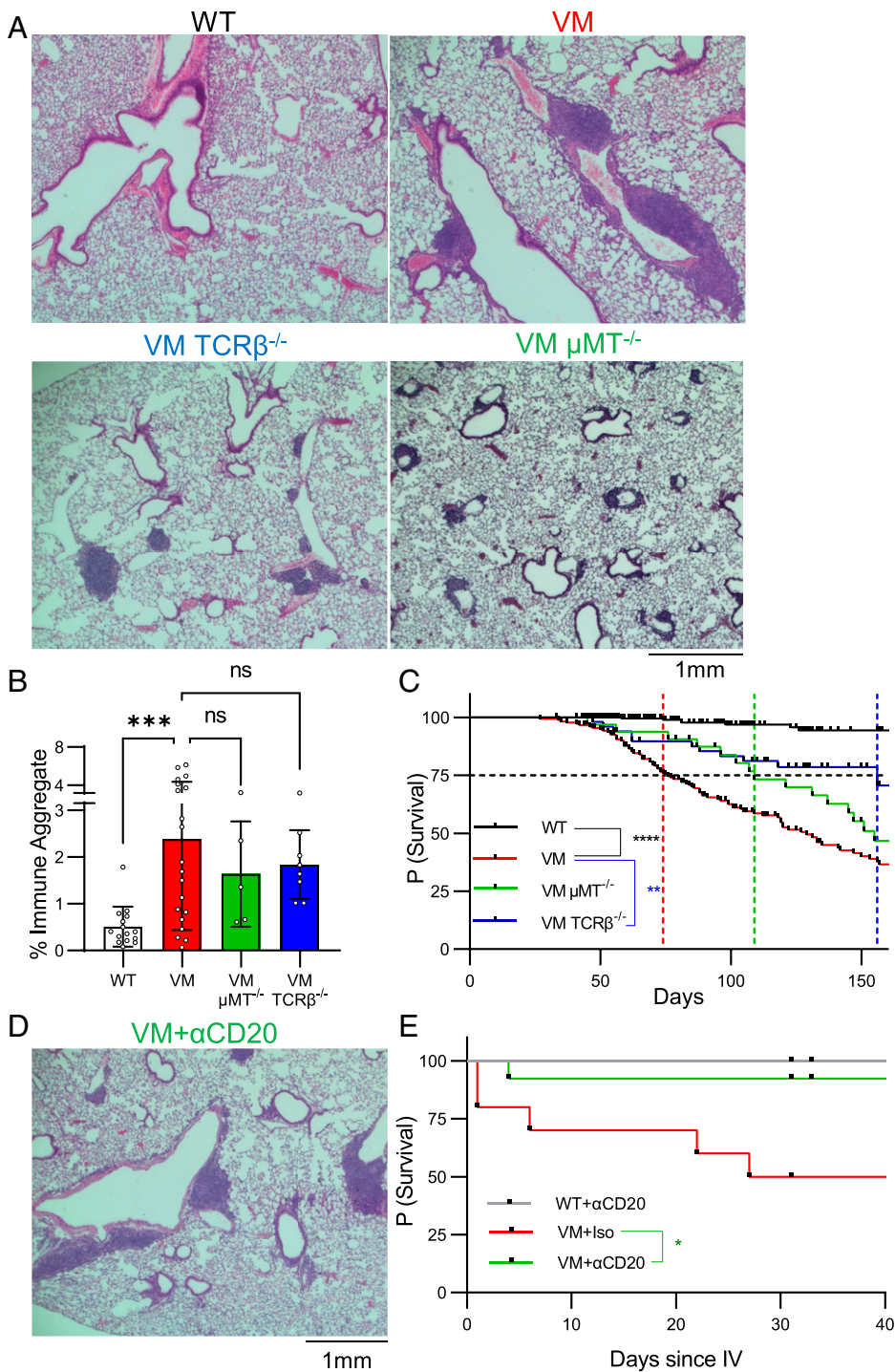
Fig. 2. B and T cells independently contribute to BALT formation and survival of VM mice. (*A*) Three- to 4-mo-old age- and sex-matched WT (*n* = 14), VM (*n* = 20), VM μMT KO (*n* = 5), and VM TCRβ KO (*n* = 8) mice were assessed by representative 4× field H&E histology from sectioned lungs. (*B*) Quantification of immune aggregates from scanned mouse lung H&E sections using a pixel classifier approach in QuPath. The percentage of immune aggregates is calculated as the fraction of pixels detected as immune aggregates over the total area of lung tissue assessed. (*C*) Kaplan–Meier survival analysis showing probability of survival over time for WT (*n* = 296), VM (*n* = 173), VM TCRβ KO (*n* = 51), and VM μMT KO (*n* = 32) mice. A black dotted line that intersects the *y* axis at 75% survival is shown. Colored lines intersecting the *x* axis are shown that represent the lifespan at which 75% of mice from each line were predicted to survive. (*C*) Six-wk-old WT and VM mice were treated with either a B cell depleting CD20 mAb (WT, *n* = 8; VM, *n* = 13) or an isotype-matched control mAb (VM, *n* = 9). Representative H&E histology from a VM mouse treated with CD20 mAb is shown. (*D*) Survival data for 6 wk following treatment as shown here by Kaplan–Meier survival curves. Nonparametric Mann–Whitney *U* tests were for pairwise comparisons, and a nonparametric Kruskal–Wallis test was used for one-way ANOVA to determine statistical significance (***P < 0.001). Statistical significance for survival was determined using a log-rank test (*P < 0.05, **P < 0.01, ****P < 0.0001).

Together, this indicates that B and αβ T cells can be independently recruited to the VM lung.

We had previously found that despite VM splenic lymphopenia, remaining lymphocytes showed significant up-regulation of activation markers (11), and we hypothesized that the lymphocytes in the VM lung would also show evidence of activation. In fact, the VM EV B cell compartment contained an increased percentage of AA4.1$^-$, IgM$^+$, IgD$^-$ cells (Fig. 4*B*, *SI Appendix*, Fig. S4*D*), indicative of a population of unswitched memory B cells identified previously in autoimmune patients and mice (16). Additionally, we observed that IgD$^+$ naive B cells in VM mice expressed high levels of the activation marker and costimulatory molecule CD86 (*SI Appendix*, Fig. S5*B*). VM EV T cells also showed an increased expression of CD69

(Fig. 4*C*) and increased proportions of CD44$^+$ CD62L$^-$ CD4 and CD8 effectors (Fig. 4*D*). Moreover, we observed that CD4 and CD8 effectors from the VM mice expressed higher levels of Tim3, a marker for short-lived effector T cells (17), and lower levels of CD127, a marker for effector memory T cells (*SI Appendix*, Fig. S5*A*). While EV αβT cells in VM μMT KO mice retained enrichment for effectors and expression of CD69 (Fig. 4 *C* and *D*), EV B cells in VM TCRβ KO mice had a lower frequency of IgD$^-$ B cells (Fig. 4*B*). These data demonstrate that αβ T cells promote the activation of B cells in the lung, but activation of αβ T cells in the lung can occur independent of B cells.

To better characterize the increased lung EV myeloid compartment in VM mice, all cells expressing either CD11b and/
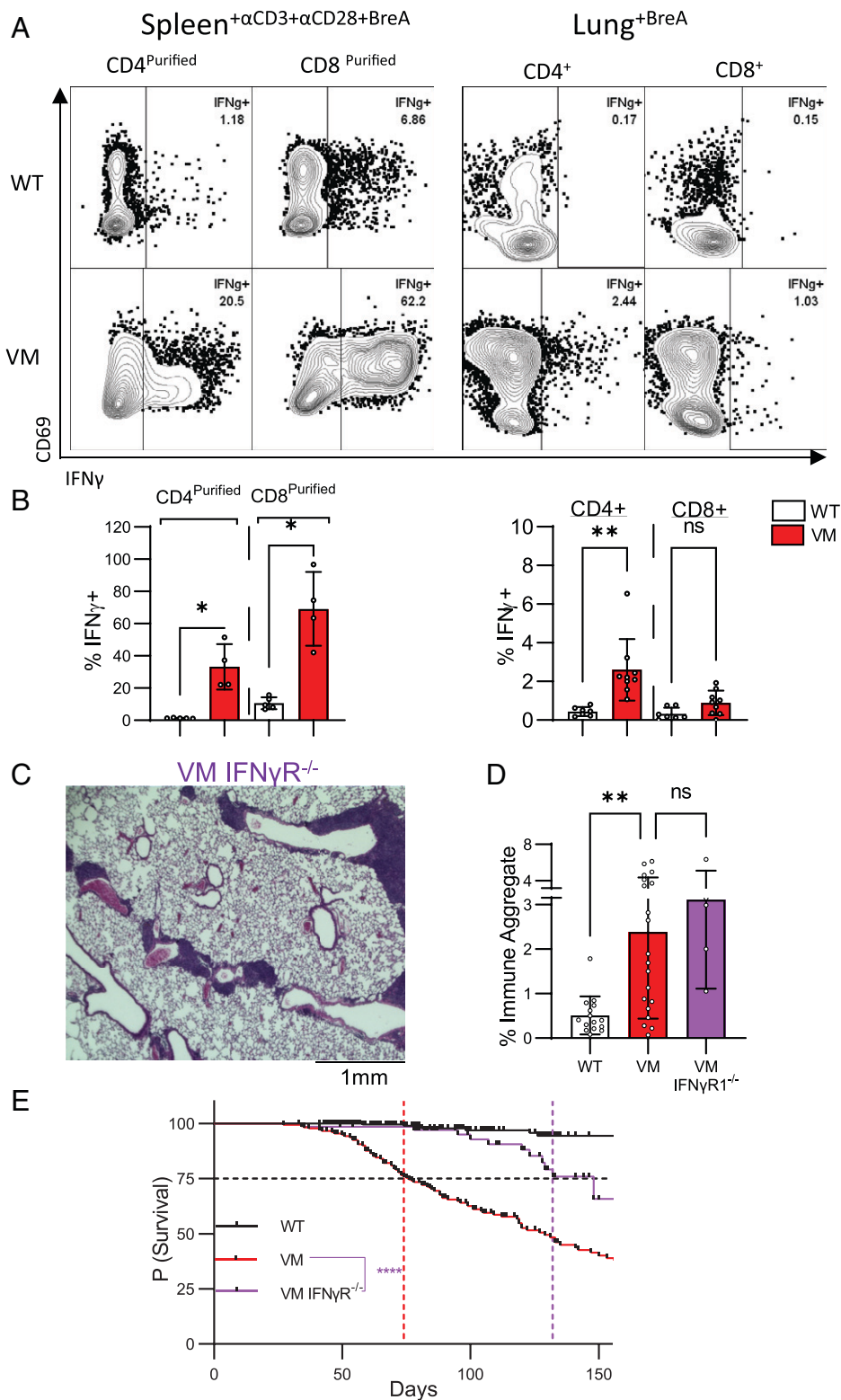
Fig. 3. VM SAVI T cells produce IFNγ, and IFNγR contributes to VM SAVI mortality. Three- to 4-mo-old age- and sex-matched WT and VM mice were assessed via IFNγ intracellular staining of magnetic bead purified CD4+ and CD8+ splenocytes stimulated with CD3 and CD28 mAb antibody overnight (WT, $n = 3$ to 4; VM, $n = 4$), and unstimulated lung suspensions (WT $n = 4$, VM $n = 5$), both treated with Brefeldin A for 4 h before assessment. Representative flow plots (*A*) and summary bar graphs are shown (*B*). (*C* and *D*) Three- to 4-mo-old age- and sex-matched WT ($n = 14$), VM ($n = 20$), and VM IFNγRKO ($n = 5$) were assessed by representative 4× field H&E histology from sectioned lungs (*C*). (*D*) Quantification of immune aggregates from scanned mouse lung H&E sections. (*E*) Kaplan–Meier survival analysis showing the probability of survival over time for WT ($n = 296$), VM ($n = 173$), and VM IFNγR KO ($n = 69$) mice. A black dotted line that intersects the *y* axis at 75% survival is shown. Colored lines intersecting the *x* axis are shown that represent the lifespan at which 75% of mice from each line were predicted to survive. Nonparametric Mann–Whitney *U* tests were for pairwise comparisons, and a nonparametric Kruskal–Wallis test was used for one-way ANOVA to determine statistical significance ($^{ns}P > 0.05$, $*P < 0.05$, $**P < 0.01$). Statistical significance for survival was determined using a log-rank test ($****P < 0.0001$).

or CD11c were further analyzed by flow cytometry. The most striking differences were the increased presence of both CD11b+Ly6G+ neutrophils and CD11b+Ly6Chi inflammatory monocytes in the VM lung (Fig. 4*E*), suggesting that the increase in lung EV myeloid cells was due to infiltration by circulating myeloid cells. Moreover, the overall increase in the total infiltrating myeloid population was dependent on αβ T cells but not B cells (Fig. 4*A*). Additionally, the percentage of

EV neutrophils in VM TCRβ KO mice was reduced compared to VM and similar to uninflamed WT, although this observation did not reach statistical significance of $P < 0.05$ (Fig. 4*E*).

Because T cells in VM mice produce IFNγ and IFNγ contributes to a reduced lifespan, we expected to find that many of the lung immune phenotypes ameliorated in VM TCRβ KO mice to also be phenocopied by VM IFNγR KO mice. In fact,
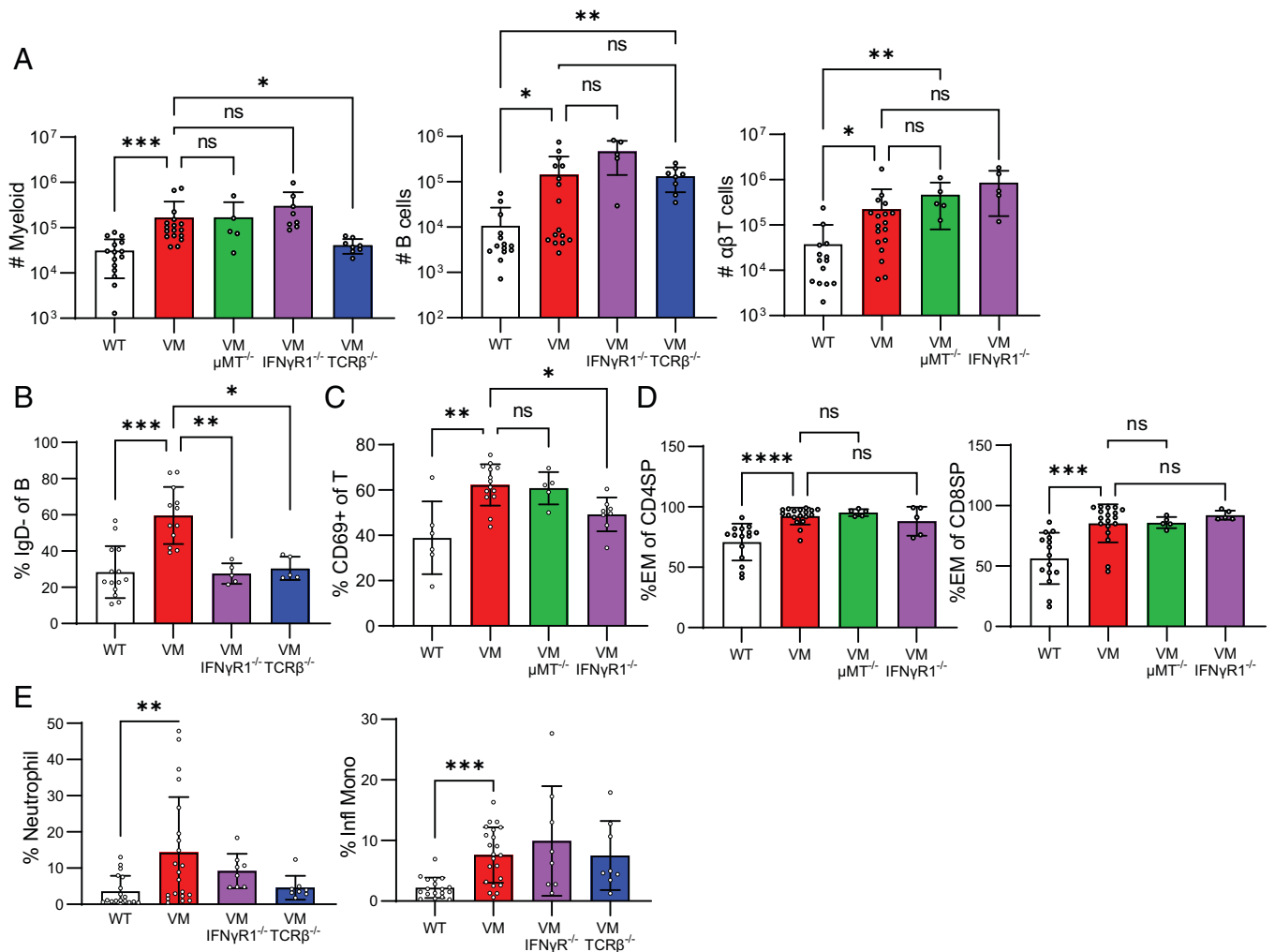
Fig. 4. VM T cells promote lung lymphocyte activation and myeloid recruitment. Three- to 4-mo-old age- and sex-matched WT ($n = 15$), VM ($n = 17$), VM TCRβKO ($n = 8$), VM μMT KO ($n = 5$), and VM IFNγRKO ($n = 8$) mice were assessed for total numbers of lung EV (CD45 IV⁻), B cells (CD19⁺B220⁺MHCII⁺), T cells (CD3⁺TCRβ⁺), and myeloid cells (CD11b⁺CD11c⁻, CD11b⁺CD11c⁺, and CD11b⁻CD11c⁺ populations) isolated from the left lung lobe and detected by flow cytometry (*A*). (*B*) Percentage of IgD⁻ B cells out of lung EV B cells (CD45 IV⁻, CD19⁺B220⁺MHCII⁺). (*C*) Percentage of CD69⁺ of lung EV αβ T cells (CD45 IV⁻ CD3⁺TCRβ⁺). (*D*) Percentage of effector subset (CD44⁺CD62L⁻) lung CD4⁺ and CD8⁺ αβ T cells assessed by flow cytometry. (*E*) Percentage of lung EV myeloid cells (CD45 IV⁻ CD11b⁺ and/or CD11c⁺) was assessed by flow cytometry for neutrophils (CD11b⁺Ly6G⁺) and inflammatory monocytes (CD11b⁺Ly6C^{hi}). Nonparametric Mann–Whitney U tests were used for pairwise comparisons, and a nonparametric Kruskal–Wallis test was used for one-way ANOVA to determine statistical significance (ⁿˢ$P > 0.05$, *$P < 0.05$, **$P < 0.01$, ***$P < 0.001$, ****$P < 0.0001$).

like VM TCRβ KO mice, VM IFNγR KO had fewer unswitched memory B cells (Fig. 4 *A* and *B*, *SI Appendix*, Fig. S4D). Additionally, while lung EV αβ T cells in the VM IFNγR KO were still enriched for effector cells (Fig. 4*D*), expression of CD69 was significantly diminished (Fig. 4*C*). However, T-cell-dependent recruitment of myeloid cells was not similarly rescued by IFNγR deficiency (Fig. 4*A*). Additionally, while infiltrating neutrophils returned to levels similar to WT, the frequency of inflammatory monocytes remained high in the VM IFNγR KO lung, although these observations did not reach statistical significance of $P < 0.05$ (Fig. 4*E*). Together, our findings demonstrate that IFNγ production by T cells promotes VM mortality and promotes activation of both T and B cells but is not required for the recruitment of B, T, or myeloid cells to the VM lung.

T cells and IFNγ Promote Proinflammatory Cytokine Production in SAVI Disease. A previous comparison of WT and VM sera by multiplex enzyme-linked immunoassay (ELISA) documented the increased production of proinflammatory cytokines and chemokines in VM mice (11). STING-driven cytokine production is often attributed to IRF3 induction of type 1 IFNs and

subsequent production of IFN-stimulated genes (18). However, IFNαR deficiency did not improve VM survival (11). Since both T cell deficiency and IFNγ deficiency improved the survival of VM mice, we predicted that many of the up-regulated inflammatory cytokines would be attributable to IFNγ and T cells but not type 1 IFNs.

To test this possibility, we compared the cytokine profiles of sera from collected from 3- to 4-mo-old VM mice and VM mice deficient for IFNαR, IFNγR, or TCRβ, by multiplex ELISA. As expected, serum cytokine levels were comparable in uninflamed WT, IFNαR KO, IFNγR KO, and TCRβ KO mice (*SI Appendix*, Fig. S6). Comparing VM to WT sera, the most significantly up-regulated cytokines (fold change > 1.75×; $p_{adj} < 0.15$) included CXCL1, CXCL10, CCL5, CCL12, CXCL9, CCL2, GM-CSF, IL-6, TNFα, and G-CSF (Fig. 5 *A* and *B*). Of these cytokines, only CXCL1 and CXCL10 were diminished by IFNαR deficiency (Fig. 5*B*, *SI Appendix*, Fig. S7A). In contrast, a much larger set of cytokines were decreased in IFNγR-deficient VM mice. These included CCL5, CCL12, CXCL9, and CCL2 (Fig. 5 *B* and *C*), in addition to CXCL1 and CXCL10 (*SI Appendix*, Fig S7A).

In line with the observation that VM T cells produce IFNγ, cytokines found to be IFNγR dependent were also largely αβ T cell dependent (Fig. 5 B and C, *SI Appendix*, Fig. S7A). Additionally, the up-regulation of the myelopoietic cytokine GM-CSF was dependent on αβ T cells but not IFNγ (*SI Appendix*, Fig. S7B). This matched the observation that the recruitment of myeloid infiltrates into the VM lung was dependent on αβ T cells but not IFNγ and suggested that T-cell-dependent GM-CSF may regulate the maintenance of myeloid cells (19–21) in the VM lung. Additionally, elevation of several cytokines in VM above the baseline of uninflamed WT mice was independent of IFNαR, IFNγR, or αβ T cells. For example, cytokines like CXCL10 and CCL12 were only found to be partially reduced in VM IFNγR KO and TCRβ KO mice (Fig. 5C, *SI Appendix*, Fig. S7A), whereas elevation of cytokines like G-CSF, IL-6, and TNFα were entirely independent of IFNαR, IFNγR, and αβ T cells (*SI Appendix*, Fig. S7C).

In summary, we found that the up-regulation of a large subset of inflammatory cytokines in VM were dependent on αβ T cells and IFNγ but not type 1 IFNs. This is consistent with attenuated mortality in TCRβ- and IFNγR-deficient, but not IFNαR-deficient, VM mice. However, the increased titers of cytokines not regulated by T cells or IFNγ suggest that inflammatory cytokines are also produced by other cell types in VM and likely include myeloid cells, stromal cells, and parenchymal cells.

SAVI Expression by CD45+ Cells Is Not Required for VM Lung Pathology. Since T cell deficiency markedly improved the survival of VM mice and led to a reduced recruitment of proinflammatory neutrophils and monocytes to the lung, we initially assumed that lymphocyte expression of the VM mutant conferred the relevant T cell effector functions that led to ILD. To better understand the role STING GOF in BM-derived hematopoietic cells, we used radiation chimeras. Lethally irradiated WT CD45.1 recipient mice, reconstituted with VM CD45.2 donor BM (VM→WT chimeras), were evaluated at 9 wk post-transplant. Despite the presence of B cells, T cells and myeloid cells in the VM→WT mice, there was minimal BALT formation in these mice as shown by lung histology (Fig. 6A) and no significant immune infiltrate by flow cytometry (Fig. 6B). We previously reported that VM donor BM cells were able to reconstitute the splenic myeloid compartment of the irradiated WT mice but poorly reconstituted the splenic B and T cell compartments (11). Similarly, in the current set of chimeras, radioresistant recipient-derived WT cells were a major component of the splenic T cell and B cell but not myeloid compartments (*SI Appendix*, Fig. S8). A similar trend was observed for the cells that infiltrated the chimeric lungs, with VM myeloid and B cells contributing poorly to the EV compartment and the complete absence of EV VM αβ T cells (Fig. 6C). However, we did observe a minor but significant decrease in survival of VM→WT chimeras, which we postulate to be secondary not to lung disease but instead due to a failure of the VM donor BM to sufficiently engraft the hematopoietic compartment (Fig. 6F).

The failure of VM→WT chimeras to develop ILD could have reflected the absence of VM-donor-derived T cells or VM-expressing radioresistant cells. To address this question, lethally irradiated VM CD45.2 mice were reconstituted with WT CD45.1 donor BM (WT→VM chimeras). Unlike the VM→WT chimeras, the WT→VM chimeras developed robust lung disease and exhibited even more extensive BALT formation (Fig. 6A), consistent with an accumulation of B cells, T cells, and myeloid cells in the lungs as shown by flow cytometry (Fig. 6B).
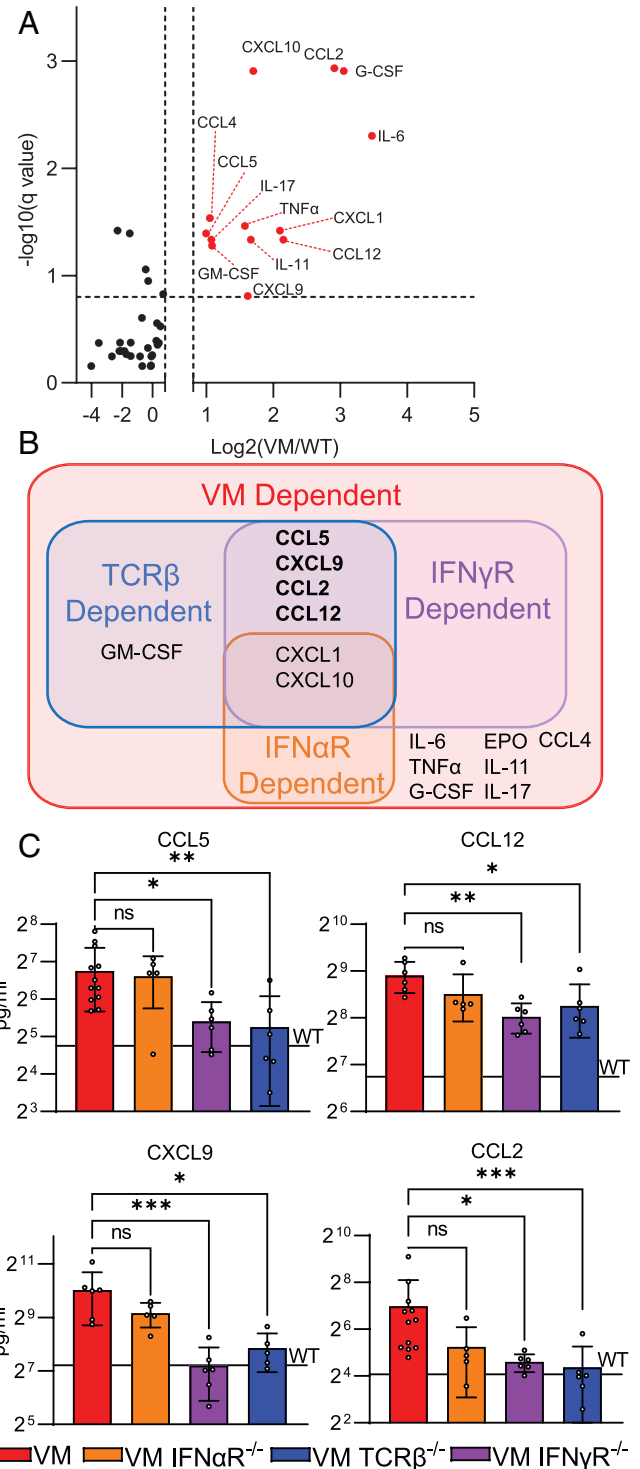

Fig. 5. T cells and IFNγ up-regulate proinflammatory cytokines in SAVI disease. Sera from 3- to 4-mo-old age- and sex-matched WT (n = 3 to 7), VM (n = 6 to 12), IFNAR KO (n = 6), VM IFNAR KO (n = 5), IFNγR KO (n = 5), VM IFNγR KO (n = 6), TCRβ KO (n = 5), and VM TCRβ KO (n = 6) mice were assessed by a multiplex Luminex ELISA for cytokine levels. (A) Volcano plot showing multiple comparisons testing of 41 analytes between WT and VM sera; analytes highlighted in red and labeled are >1.75× elevated in VM with an adjusted P value of <0.15. (B) Venn diagram showing the overlap of sera analytes up-regulated in VM, VM IFNαR KO, VM IFNγR KO, and VM TCRβ KO compared to WT controls. (C) Sera analytes down-regulated in VM IFNγR KO and VM TCRβ KO compared to VM. For C, the black line labeled "WT" represents the average level of the cytokine detected in the sera of WT control samples. Multiple -comparison testing was performed as nonparametric multiple-Mann–Whitney U testing with a false discovery rate of 25%. Nonparametric Kruskal–Wallis test was used for one-way ANOVA to determine statistical significance (nsP > 0.05, *P < 0.05, **P < 0.01, ***P < 0.001).
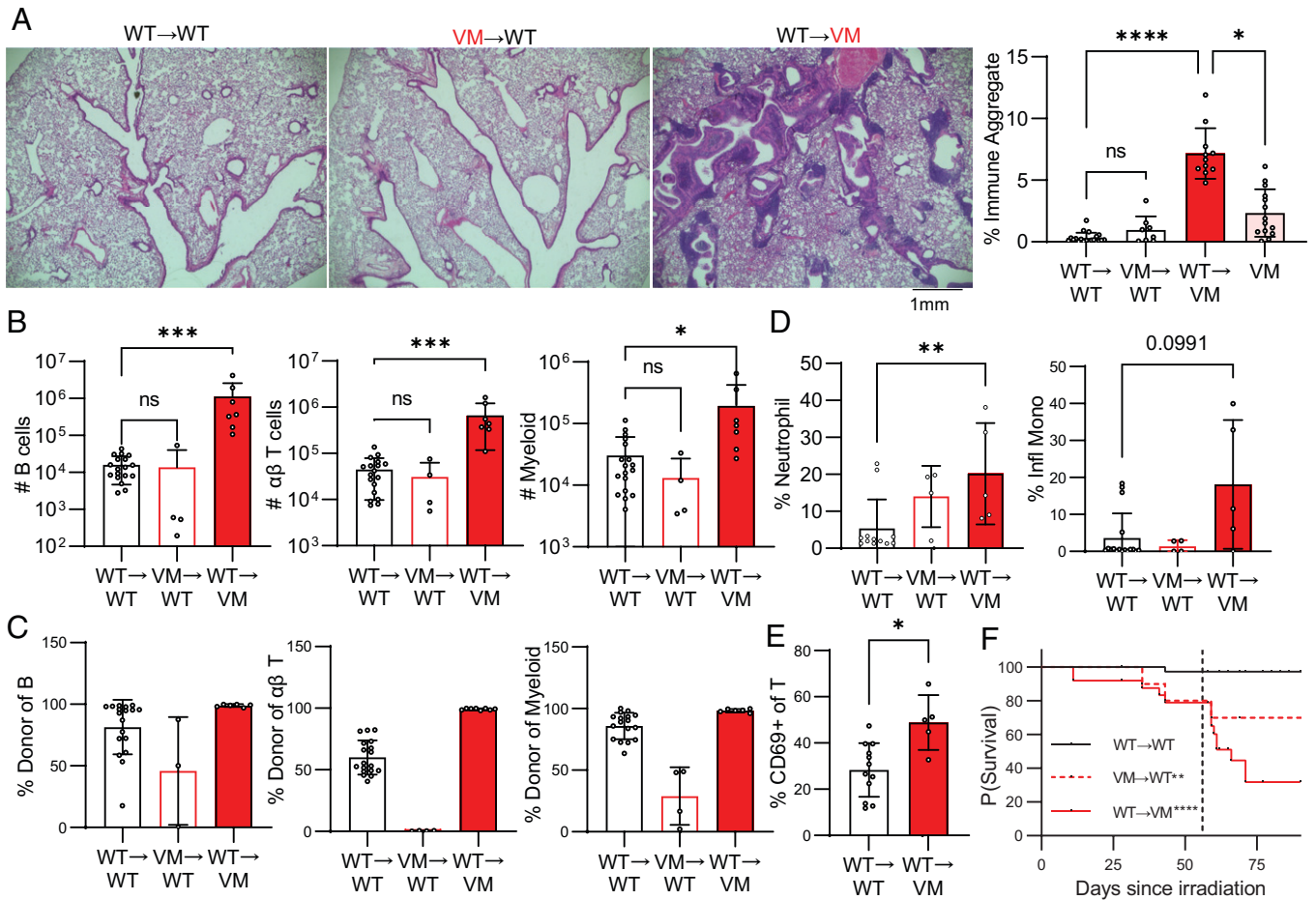
Fig. 6. SAVI-expressing CD45$^+$ cells are not required for VM BALT pathology. WT and VM mice were lethally irradiated at 6 wk of age and then reconstituted with donor BM to generate WT→WT ($n = 18$), VM→WT ($n = 4$ to 11), and WT→VM ($n = 7$ to 11) chimeric mice and assessed 9 wk later. (A) Representative H&E histology of lungs from WT→WT, VM→WT, and WT→VM chimera lungs, and the quantification of percent immune aggregates is as described above. (B) Total numbers of lung EV (CD45 IV$^-$) B cells (CD19$^+$B220$^+$MHCII$^+$), T cells (CD3$^+$TCRβ$^+$), and myeloid cells (CD11b$^+$ and/or CD11c$^+$) cells assessed by flow cytometry. (C) Percentage of engrafted EV B, αβ T, and myeloid cells in the lung that were derived from donor cells as determined by flow cytometry. (D) Percentage of donor lung EV myeloid cells (CD45 IV$^-$ CD11b$^+$ and/or CD11c$^+$) that were neutrophils (CD11b$^+$Ly6G$^+$) and inflammatory monocytes (CD11b$^+$Ly6-C^{hi}). (E) Percent CD69$^+$ of donor lung EV αβ T cells (CD45 IV$^-$ CD3$^+$TCRβ$^+$). (F) Kaplan–Meier survival curves for WT→WT ($n = 38$), VM→WT ($n = 10$), and WT→VM ($n = 25$). A black dotted line that intersects the x axis at 56 d is shown, indicating the time that engraftment of donor BM was expected to have been completed. Nonparametric Mann–Whitney U tests were used for pairwise comparisons, and a nonparametric Kruskal–Wallis test was used for one-way ANOVA to determine statistical significance ($^{ns}P > 0.05$, $^*P < 0.05$, $^{**}P < 0.01$, $^{***}P < 0.001$, $^{****}P < 0.0001$). Statistical significance for survival was determined using a log-rank test ($^{**}P < 0.01$, $^{****}P < 0.0001$).

Importantly, VM CD45.2$^+$ radioresistant cells were not detected in either the spleen (*SI Appendix*, Fig. S8) or lungs (Fig. 6C) of WT→VM chimeras. Thus, it was unlikely that radioresistant CD45$^+$ VM cells reinitiated ILD. Other similarities between the WT→VM chimeras and VM EV lung cells included activated T cells, enrichment for neutrophils, and enrichment for inflammatory monocytes, although this latter observation did not reach the statistical cutoff of $P < 0.05$ ($P = 0.0991$) (Fig. 6 D and E). Furthermore, WT→VM chimeras showed a dramatic increase in mortality that was notably exacerbated at 8 wk post-BM transfer, suggesting that engraftment of WT donor immune cells is sufficient for the development of lung pathology and mortality (Fig. 6F).

It is known that irradiation can initiate lung inflammation and fibrosis in both man and mouse (22, 23). To rule out potential radiation artifacts in the development of disease in WT→VM chimeras, we generated chimeric mice using the chemotherapeutic agent busulfan to deplete hematopoietic stem cells. Consistent with WT→VM radiation chimeras, WT→VM busulfan chimeras also developed BALT (*SI Appendix*, Fig. S9A), accumulation of EV immune cells (*SI Appendix*, Fig. S9B), and features of immune activation (*SI Appendix*, Fig. S9D), although due to our

small sample size, these findings did not reach statistical significance. Importantly, 95% of CD45$^+$ cells in the lungs of WT→VM busulfan chimeras were donor derived, indicating a minimal contribution from busulfan-resistant VM CD45$^+$ cells (*SI Appendix*, Fig. S9C). These results further demonstrate that VM CD45$^+$ cells are not required for the development of BALT pathology in VM mice. Instead, stromal and/or parenchymal cells expressing the VM mutation robustly promote BALT pathology, and WT BM-derived cells are recruited to the VM lung as activated lymphocytes and infiltrating myeloid cells, recapitulating the phenotype of unmanipulated VM SAVI.

SAVI Lung Endothelial Cells Express STING and Show a Transcriptomic Signature Indicating Activation and Elevated Immune Function. SAVI, as its name suggests, is associated with significant small vessel vascular pathology (6–8), suggesting VM endothelial cells are involved in pathogenesis. Endothelial cell STING expression has been noted in several single-cell RNA and protein atlases for both mice and humans (24, 25). To confirm the expression of STING in mouse lung endothelial cells, we isolated RNA from sorted WT and VM CD31$^+$ lung cells and performed bulk RNA sequencing (RNAseq). Comparable levels of
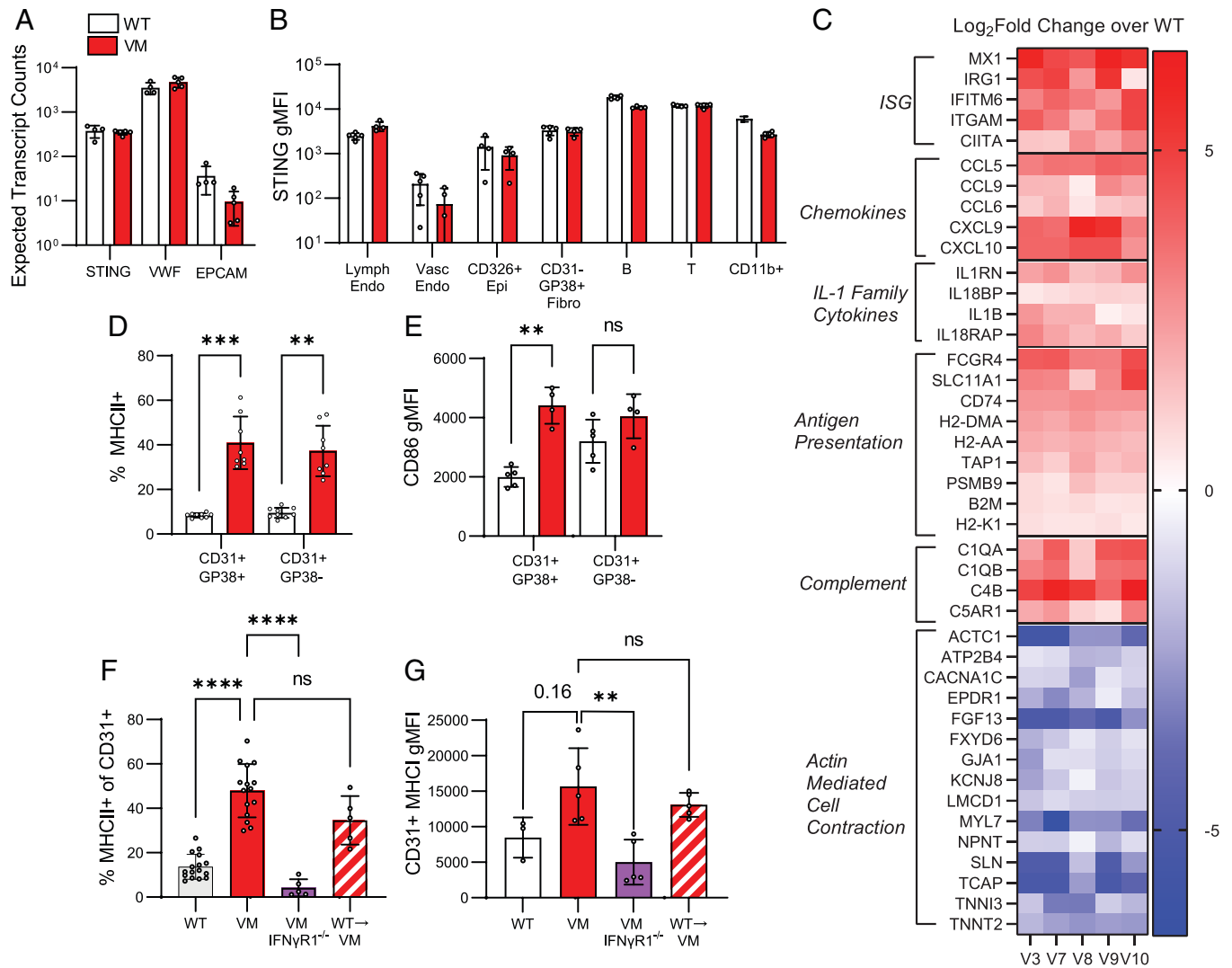
Fig. 7. SAVI lung endothelial cells express STING and show the gene signature indicating activation and elevated immune function. (A) Expected transcript counts for STING, VWF (Endothelial marker gene), and EPCAM (epithelial marker gene) from bulk RNAseq of sorted lung endothelial cells (CD31$^+$CD45$^-$CD326$^-$CD140a$^-$Ter119$^-$) from WT ($n = 4$) and VM ($n = 5$) mice. (B) Intracellular staining for STING was performed on perfused and elastase digested lungs from WT ($n = 5$), VM ($n = 4$), and STING KO ($n = 1$). We report STING geometric mean fluorescence intensity (gMFI) of WT and VM lung in specific populations above the baseline STING gMFI measured in the same population identified in a STING KO control sample. The populations we show are lymphatic endothelia (CD45$^-$CD326$^-$CD31$^+$CD38$^+$), vascular endothelia (CD45$^-$CD326$^-$CD31$^+$CD38$^-$), epithelia (CD45$^-$CD31$^-$CD326$^+$), fibroblasts (CD45$^-$CD31$^-$CD326$^-$GP38$^+$), B cells (CD45$^+$B220$^+$MHCII$^+$CD3$^-$CD11b$^-$), T cells (CD45$^+$CD3$^+$B220$^-$CD11b$^-$), and myeloid cells (CD45$^+$CD11b$^+$CD3$^-$B220$^-$). (C) Heatmap of selected differentially expressed genes from bulk RNAseq of sorted VM ($n = 5$) lung endothelia compared to WT ($n = 4$) controls, expressed as the log$_2$ fold change of gene expression of VM samples compared to the average WT value. Genes are grouped by functional or ontological classification and by whether they are up- (shown as red) or down- (shown as blue) regulated. Percentage of MHCII expression (D) and gMFI (E) for surface CD86 was measured for lymphatic endothelia and vascular endothelia in elastase digested WT and VM lungs. (F) Percentage of MHCII expression was measured for CD31$^+$ lung endothelia in WT ($n = 16$), VM (n = 15), VM IFNγR KO ($n = 5$), and WT→VM chimeric mice ($n = 5$). (G) Surface MHCI (H2/kb) gMFI for CD31$^+$ endothelial cells from WT ($n = 3$), VM ($n = 5$), VM IFNγR KO ($n = 5$), and WT→VM chimeric mice ($n = 5$). Nonparametric Mann–Whitney U tests were used for pairwise comparisons, and a nonparametric Kruskal–Wallis test was used for one-way ANOVA to determine statistical significance ($^{ns}P > 0.05$, $^{**}P < 0.01$, $^{***}P < 0.001$, $^{****}P < 0.0001$).

the STING transcript were detected in lung endothelial cells from both strains and were higher than nonendothelial markers like EPCAM, although lower than endothelial associated markers like VWF (Fig. 7*A*). We further evaluated STING expression by flow cytometry, comparing lung suspensions from WT and STING-deficient mice. STING expression was detected in lung-resident immune cells including B, T, and myeloid cells (Fig. 7*B*), consistent with previous literature demonstrating that STING is ubiquitously expressed in both lymphocytes and myeloid cells (26). Among the CD45$^-$ stromal and parenchymal lung cells, WT CD326$^+$ epithelia, CD31$^+$ endothelia, and CD31$^-$CD326$^-$GP38$^+$ fibroblasts all expressed STING above the level of their respective STING KO control populations but expressed less STING overall than CD45$^+$ hematopoietic-derived cells (Fig. 7*B*). Moreover, we were able to stratify CD31$^+$GP38$^+$

lymphatic endothelium and CD31$^+$ GP38$^-$ vascular endothelia and showed that both express STING.

To assess the phenotype of lung endothelial cells in VM mice, we further analyzed bulk RNAseq from sorted CD31$^+$ WT and VM lungs and observed robust changes in the transcriptomic profile of VM lung endothelial cells indicative of an elevated immune response. Differential gene expression analysis identified 237 genes that were significantly up-regulated (p$_{adj}$ < 0.1) in VM endothelia by at least twofold, and 83 genes that were significantly down-regulated by at least twofold (*SI Appendix*, Fig. S10*A*). Gene ontology analysis of the up-regulated genes identified terms related to immune function including antigen presentation, chemotaxis, and IFN responses as significantly enriched (*SI Appendix*, Fig. S10*B*). Up-regulated genes included ISGs, chemokines, IL-1 family cytokines, antigen presentation, and complement genes, and representative genes are shown

(Fig. 7C). In contrast, gene ontology of down-regulated genes identified terms primarily related to actin-mediated cell contraction (*SI Appendix*, Fig. S10B), and representative genes are shown (Fig. 7C).

To confirm that gene transcription related to antigen presentation reflected a protein-level phenotype, we assessed WT and VM lung endothelial cells by flow cytometry. MHCII (IA/IE) was significantly up-regulated on both lymphatic and vascular VM endothelia (Fig. 7D), and the costimulatory marker CD86 was up-regulated on lymphatic endothelium (Fig. 7E). Overall, these data demonstrate that lung endothelial cells express STING and that VM endothelia have the potential for enhanced immune function.

IFNγR is ubiquitously expressed by hematopoietic, stromal, and parenchymal cells, and stimulation of endothelial cells by IFNγ has been shown to enhance endothelial activation and antigen presentation (27, 28). To determine whether IFNγ contributed to the up-regulation of MHCII on VM lung endothelial cells, we compared MHCII expression in VM and VM IFNγR KO cells and found that MHCII was dramatically reduced on VM IFNγR KO endothelial cells (Fig. 7F). MHCII was also up-regulated on lung endothelial cells from WT→VM chimera mice (Fig. 7F), which feature a population of activated tissue-resident T cells. Moreover, MHC I (H2-kb) was up-regulated on VM endothelial populations, although this finding did not reach statistical significance of $P < 0.05$ compared to WT ($P = 0.16$) (Fig. 7G). However, endothelial expression of MHCI was significantly attenuated in VM IFNγR KO mice compared to VM and remained elevated in WT→VM chimera mice. Overall, these data suggest that up-regulation of endothelial cell MHCII in the VM lung is regulated by IFNγ-producing T cells recruited to the lung by radioresistant stromal and parenchymal cells.

Discussion

In this study, we examined the pulmonary inflammation and pathology resulting from STING VM GOF mutations in mice by using a combination of histological, flow cytometric, and functional approaches. We conclude that VM mice develop a form of restrictive ILD best described as FB or LIP, with significant parallels to the lung disease described for pediatric SAVI patients. We further demonstrated a key role for αβ T cells in the development of lung pathology that partially depends on the production of IFNγ. However, inherent expression of the VM mutation by T cells is not required. Rather, nonhematopoietic cells expressing the VM mutation are sufficient for pulmonary BALT development, T cell activation, and reduced lifespan.

The BALT in VM mice appeared to correspond to nodules visible on micro-CT, a CT finding also noted in human SAVI patients (6). VM SAVI mice also recapitulate neutrophilic alveolitis frequently observed in SAVI patients (6), as well as restrictive pulmonary dysfunction (6, 29). Despite these similarities, differences exist between VM mice and SAVI patients. SAVI patient lung CTs often reveal the presence of cysts and ground glass opacities, which we did not observe in murine VM micro-CT studies, potentially due to additional exacerbating environmental exposures of SAVI patients. VM mice also frequently develop milky pleural effusions, which have not been reported in SAVI patients but that are reported in other CTD-ILD as a result of cholesterol or chylous lymphatic effusions (30–32).

In general, VM mice develop a more robust disease phenotype than other gene-targeted SAVI lines, including the commonly studied NS mutation, as indicated by shorter lifespan, frequency of mutant offspring, severity of lung disease, and extent of B cell lymphopenia (11). Accordingly, B cells appear to play a more prominent role in our studies of VM ILD than previously reported for the NS model (12), as activated B cells accumulate in VM BALT and B cell depletion significantly improves survival. This suggests that different SAVI mutations promote pathology through activation of distinct immune populations.

Our studies demonstrate a more prominent role for T cells than B cells in the development of ILD. T cells promote the accumulation of myeloid cells to the VM lung, lead to the production of inflammatory cytokines, and contribute to mortality. Moreover, we identified IFNγ production as an effector mechanism that can account for many of the T-cell-dependent phenotypes observed in VM SAVI. Although other cell types besides αβ T cells, such as natural killer cells and ILCs, can contribute to IFNγ production, our data support T-cell-derived IFNγ as the most likely explanation for our findings. We speculate that activated IFNγ-producing T cells accrue in the VM SAVI lung due to enhanced self-reactivity. Indeed, NS SAVI mice with a restricted TCR repertoire, due to expression of the OT-I transgenic TCR, develop much less severe systemic inflammation and lung pathology than NS mice (13). However, OT-I mice are deficient in CD4 T cells, and this may also contribute to attenuated pathology in NS OT-I mice. Consistent with a role for CD4 T cells in SAVI lung pathology, our findings show that VM lung CD4 T cells produce more IFNγ than lung CD8 T cells. Our future studies will seek to clarify the role of CD4 and CD8 T cell autoreactivity in SAVI lung disease.

The formation of BALT requires complex interactions between hematopoietic immune cells and stromal tissues and involves multiple parallel cytokine and chemokine pathways (33). Thus, it is often unclear whether the initiation of BALT results from hematopoietic or stromal/parenchymal responses to inflammatory stimuli. Despite the major role of lymphocytes in VM lung disease, our radiation chimera studies show that the expression of the VM mutation by BM-derived cells was not required for BALT pathology. Rather, VM mouse lung stromal and parenchymal cells not only express STING but also recruit WT (non-STING GOF) immune cells to form BALT. We propose that the recruitment of immune cells depends on the inherent expression of the VM mutation by stromal and/or parenchymal cells. However, we cannot rule out that factors independent of direct STING GOF modify the lung environment prior to irradiation. The dependence on radioresistant host cells in the VM lung model contrasts with the spontaneous colitis that arises in NS SAVI mice, where T cells, again either GOF or WT, are required for gut pathology, but GOF myeloid cells serve as the initiators of the disease process (34). SAVI patients show diverse, tissue-specific manifestations of disease, and therapeutic management of autoinflammation in the skin, lungs, or other tissues of SAVI patients may need to be directed toward distinct initiating cell populations.

Additionally, BALT pathology and the number of lung EV B and T lymphocytes in WT→VM chimeras was more severe than in the original VM SAVI mice. This corresponds to a dramatic increased rate of mortality at 8 wk posttransplantation. We speculate that this reflects the improved survival of WT lymphocytes compared to VM lymphocytes, where expression of STING GOF mutations promotes cell death as a result of elevated endoplasmic reticulum stress (13). Thus, VM SAVI disease may be exacerbated by the increased presence of lymphocytes that do not have an intrinsic impairment in survival.

Among a wide range of monogenic interferonopathies, only SAVI and COPA patients develop lung disease (35, 36). Both of

these diseases are driven by activation of STING (36, 37), suggesting that the lung may be particularly sensitive to STING-induced pathology. Intriguingly, across all organs surveyed in human data sets, STING is most highly expressed in the lung (25), and single-cell RNAseq and immunohistochemistry further demonstrate that STING is expressed in hematopoietic, stromal, and parenchymal tissues of the lung in mice and men (24, 25). While STING has been most well characterized in hematopoietic cells, STING clearly plays a functional role in the regulation of inflammation by stromal and parenchymal cell types. For example, antitumorigenic STING agonists can induce endothelial cells to secrete cytokines (38) and maintain barrier integrity to prevent metastasis (39). Additionally, recent studies support a role for lung endothelial STING activation in severe COVID lung pathology (40). The lung is highly vascularized, requiring vascular endothelia to mediate gas exchange, as well as lymphatic endothelia to sample antigens. Vasculopathy of small capillaries is a key finding in SAVI patients (7), and the lung is the largest capillary bed in the body. Therefore, we reasoned endothelial cells may contribute to lung pathology in SAVI disease.

Endothelial cells express functional pattern recognition receptors and serve immunologic functions such as antigen presentation and production of proinflammatory cytokines and chemokines (27, 28, 41). Consistent with a potential role for endothelial cells in SAVI lung autoinflammation, our transcriptional and flow cytometric data demonstrate that endothelial cells from VM mice up-regulate surface expression of MHCII and CD86, as well as other genes related to antigen presentation, chemotaxis, IL-1 family cytokines, and complement. Although antigen presentation by endothelial cells is typically thought to promote self-tolerance through the induction of regulatory T cells and formation of quiescent memory (42, 43), endothelial cell antigen presentation can also enhance tissue damage under conditions of inflammation (27). Our future experiments will use genetic models to define the role of endothelial antigen presentation in SAVI lung autoinflammation. Moreover, our data demonstrate that STING is expressed by other stromal and parenchymal cells in the lung, including fibroblasts and epithelial cells. Indeed, epithelial cells and fibroblasts secrete inflammatory cytokines in response to STING agonists (44–46); thus, our future work will also seek to determine whether other stromal and parenchymal populations beyond endothelial cells might also contribute to SAVI lung pathology.

We find that SAVI ILD involves initiation by stromal and parenchymal cells and exacerbation by adaptive immunity, implicating targetable underlying mechanisms that may be shared across CTD-ILD subtypes. One interventional strategy is to mitigate the adaptive response central to disease, and we propose that SAVI patients may benefit from a combined depletion of both B and T cells as well as IFNγ-blocking regimens (47–51). Because SAVI disease up-regulates several proinflammatory cytokine pathways, much attention has been given to JAK-STAT inhibitors that block signaling common to a multitude of cytokine receptors, including IFNγR (6, 52). However, SAVI ILD is recalcitrant to JAK inhibitors (6), potentially resulting from off-target effects on protective cytokine pathways, and targeted blockade of the IFNγR may prove to be more efficacious. Therapeutic strategies to target lung stromal and parenchymal cells should also be explored for the treatment of SAVI ILD. For example, we postulate that lung transplantation would prevent the subsequent reinitiation of lung disease in SAVI patients, although there may be potential for reinitiation of disease by residual activated T cells or revascularization of transplant tissue with SAVI-expressing endothelial cells. Additionally, complications following lung transplantation are common (53) and

require maintenance of tolerance by immunosuppressive agents. Thus, additional work is needed to identify specific stromal and parenchymal initiating factors and develop targeted therapeutics against SAVI ILD. In conclusion, our findings suggest that the interplay between lymphocytes and stromal/parenchymal cells is critical for the development of SAVI ILD, and the mechanisms that support such interactions warrant further investigation.

Materials and Methods

Mice. STING VM SAVI mice were generated as described (11). SAVI VM mice and WT littermate controls were generated by crossing heterozygous male mice with WT females. IFNAR KO mice were provided by Dr. J. Sprent (Scripps, La Jolla, CA) (54). STING KO mice fully backcrossed to the C57BL/6 background were kindly provided by Dr. D. Stetson (University of Washington, Seattle, WA) (55). IFNγR KO, TCRβ KO, TCRβ KO TCRδ KO, and μMT KO mice were obtained from The Jackson Laboratory. VM mice were intercrossed with IFNαR KO, IFNγR KO, TCRβ KO, TCRβ KO TCRδ KO, and μMT KO mice to generate each respective VM KO mouse line and were maintained by true breeding for the KO genes. All mice used in these experiments were maintained in the same room and racks. STING$^{VM/WT}$ (VM) and STING$^{WT/WT}$ (WT) littermate- and sex-matched controls were used for all experiments and to generate survival curves. Roughly equal numbers of male and female mice were used. The spontaneous death of mice was tracked until 5 mo of age to generate Kaplan–Meier survival curves and survival between VM gene-of-interest KO mouse lines were compared to VM mice. Mice were euthanized by isoflurane followed by cervical dislocation prior to harvesting the lung. Serum was collected by cardiac puncture of euthanized animals. BALF was collected using ice cold Dulbecco's phosphate-buffered saline, and a flexible i.v. catheter. All animal experiments were conducted in accordance with the Institutional Animal Care and Use Committees at the University of Massachusetts Chan Medical School.

Histology. Lungs were dissected, inflated intratracheally with 10% phosphate buffered formalin (PBF) via a flexible catheter, fixed in 10% PBF at room temperature for 48 h, transferred into 70% EtOH, paraffin embedded, sectioned, and then stained by hematoxylin and eosin (H&E). Whole H&E lung slides were scanned at 4× using an EVOS FL Auto microscope. Whole slide images were then analyzed in QuPath (56) using trained pixel classifiers, namely, one trained to identify tissue broadly and another trained to specifically identify immune aggregates. Briefly, lung images were first annotated to remove any incidental heart or other nonlung tissue that was present in the section. A pixel classifier was then used to identify the total area of lung tissue in this annotation, and then a subsequent pixel classifier identified the fraction of the lung tissue that contained immune aggregates. The immune aggregates are expressed as a percentage of the total lung tissue area analyzed.

Flow Cytometry. Cells were incubated in CD16/32 (Biocell #BE0307) and stained with antibodies as documented in *SI Appendix*, Table S1. Samples were fixed using Fluorofix buffer (Biolegend #422101). Intracellular staining was performed using a BD Biosciences Fixation/Permeabilization kit (BD Biosciences #554714) after stimulating cells for 4 h with Brefeldin A (Biolegend #420601). Absolute cell counts were determined using counting beads (Biolegend #424902). Cells were acquired on an LSRII (BD Biosciences) or an Aurora (Cytek) cytometer and analyzed with FlowJo software.

RNASeq. Lungs were digested by GentleMACS as described above, stained with antibodies, and sorted for CD31$^+$CD326$^-$CD140a$^-$CD45$^-$ cells using a FACSAriaII instrument (BD Biosciences) into RLT buffer (Qiagen #79216) with betamercaptoethanol. Lysed cells were then shipped to BGI Genomics for RNA isolation, library preparation, and sequencing. FASTA sequencing files were then analyzed using a standard RNAseq pipeline (DolphinNext) (57) to perform sequence alignment (STAR), differentially expressed gene identification (DESeq2), and data visualization (DEBrowser). Differentially expressed genes were then further assessed by gene ontology (gProfiler) and by pathway enrichment analysis (EnrichmentMap) (58). Raw sequencing data are available in the Gene Expression Omnibus under accession code GSE196342.

Cytokine Analysis. Cytokine levels in mouse serum were measured by multiplex protein analysis by EveTechnologies using their 31-plex Discovery Assay

array (MD31) and their 44-plex discovery assay array (MD44). Additional ELISAs for IFNγ, IL-4, IL-17, and TNFα from primary T cell culture supernatants were performed as previously described (59).

Data Availability. RNA seq data have been deposited in GEO (GSE196342). All study data are included in the article and/or SI Appendix.

Author affiliations: [a]Program in Innate Immunity, Department of Medicine, University of Massachusetts Chan Medical School, Worcester, MA 01605; [b]Division of Rheumatology, Department of Medicine, University of Massachusetts Chan Medical School, Worcester, MA 01605; [c]Department of Immunology, Duke University School of Medicine, Durham, NC 22710; and [d]Department Pediatrics, Duke University School of Medicine, Durham, NC 22710

1. C. Vacchi et al., Therapeutic options for the treatment of interstitial lung disease related to connective tissue diseases. A narrative review. J. Clin. Med. 9, 407 (2020).
2. B. Duchemann et al., Prevalence and incidence of interstitial lung diseases in a multi-ethnic county of Greater Paris. Eur. Respir. J. 50, 1602419 (2017).
3. F. J. Martinez et al., Idiopathic pulmonary fibrosis. Nat. Rev. Dis. Primers 3, 17074 (2017).
4. H. Yoo et al., Connective tissue disease-related interstitial lung disease (CTD-ILD) and interstitial lung abnormality (ILA): Evolving concept of CT findings, pathology and management. Eur. J. Radiol. Open 8, 100311 (2020).
5. H. Kim, G. A. M. Sanchez, R. Goldbach-Mansky, Insights from Mendelian interferonopathies: Comparison of CANDLE, SAVI with AGS, monogenic lupus. J. Mol. Med. (Berl.) 94, 1111–1127 (2016).
6. M. L. Frémond et al., Overview of STING-associated vasculopathy with onset in infancy (SAVI) among 21 patients. J. Allergy Clin. Immunol. Pract. 9, 803–818.e11 (2021).
7. Y. Liu et al., Activated STING in a vascular and pulmonary syndrome. N. Engl. J. Med. 371, 507–518 (2014).
8. C. Picard et al., Severe pulmonary fibrosis as the first manifestation of interferonopathy (TMEM173 mutation). Chest 150, e65–e71 (2016).
9. J. D. Warner et al., STING-associated vasculopathy develops independently of IRF3 in mice. J. Exp. Med. 214, 3279–3292 (2017).
10. D. Bouis et al., Severe combined immunodeficiency in stimulator of interferon genes (STING) V154M/wild-type mice. J. Allergy Clin. Immunol. 143, 712–725.e5 (2018).
11. M. Motwani et al., Hierarchy of clinical manifestations in SAVI N153S and V154M mouse models. Proc. Natl. Acad. Sci. U.S.A. 116, 7941–7950 (2019).
12. H. Luksch et al., STING-associated lung disease in mice relies on T cells but not type I interferon. J. Allergy Clin. Immunol. 144, 254–266.e8 (2019).
13. J. Wu et al., STING-mediated disruption of calcium homeostasis chronically activates ER stress and primes T cell death. J. Exp. Med. 216, 867–883 (2019).
14. J. Rangel-Moreno et al., Inducible bronchus-associated lymphoid tissue (iBALT) in patients with pulmonary complications of rheumatoid arthritis. J. Clin. Invest. 116, 3183–3194 (2006).
15. A. Sirajuddin et al., Primary pulmonary lymphoid lesions: Radiologic and pathologic findings. Radiographics 36, 53–70 (2016).
16. I. Sanz et al., Challenges and opportunities for consistent classification of human B cell and plasma cell populations. Front. Immunol. 10, 2458 (2019).
17. L. Avery, J. Filderman, A. L. Szymczak-Workman, L. P. Kane, Tim-3 co-stimulation promotes short-lived effector T cells, restricts memory precursors, and is dispensable for T cell exhaustion. Proc. Natl. Acad. Sci. U.S.A. 115, 2455–2460 (2018).
18. M. Motwani, S. Pesiridis, K. A. Fitzgerald, DNA sensing by the cGAS-STING pathway in health and disease. Nat. Rev. Genet. 20, 657–674 (2019).
19. Y. Shibata et al., GM-CSF regulates alveolar macrophage differentiation and innate immunity in the lung through PU.1. Immunity 15, 557–567 (2001).
20. J. A. Hamilton, J. A. Hamilton, GM-CSF in inflammation. J. Exp. Med. 217, e20190945 (2020).
21. J. Gschwend et al., Alveolar macrophages rely on GM-CSF from alveolar epithelial type 2 cells before and after birth. J. Exp. Med. 218, e20210745 (2021).
22. K. R. Olivier, T. Peikert, D. Owen. "Radiation-induced lung injury" in UpToDate (ed. J. R. Jett, S. E. Schild, Ed.) (Wolters Kluwer, 2022).
23. M. Ghita et al., Preclinical models of radiation-induced lung damage: Challenges and opportunities for small animal radiotherapy. Br. J. Radiol. 92, 20180473 (2019).
24. N. Schaum et al.; Tabula Muris Consortium; Overall coordination; Logistical coordination; Organ collection and processing; Library preparation and sequencing; Computational data analysis; Cell type annotation; Writing group; Supplemental text writing group; Principal investigators, Single-cell transcriptomics of 20 mouse organs creates a Tabula Muris. Nature 562, 367–372 (2018).
25. A. Digre, C. Lindskog, The Human Protein Atlas-spatial localization of the human proteome in health and disease. Protein Sci. 30, 218–233 (2021).
26. M. F. Gulen et al., Signalling strength determines proapoptotic functions of STING. Nat. Commun. 8, 427 (2017).
27. C. Claser et al., Lung endothelial cell antigen cross-presentation to CD8+T cells drives malaria-associated lung injury. Nat. Commun. 10, 4241 (2019).
28. J. Mai, A. Virtue, J. Shen, H. Wang, X. F. Yang, An evolving new paradigm: Endothelial cells–Conditional innate immune cells. J. Hematol. Oncol. 6, 61 (2013).
29. A. A. de Jesus, R. Goldbach-Mansky, Genetically defined autoinflammatory diseases. Oral Dis. 22, 591–604 (2016).
30. J. E. Heffner, "Etiology, clinical presentation, and diagnosis of chylothorax" in UpToDate, V. C. Broaddus, Ed. (Wolters Kluwer, 2022).
31. J. E. Heffner, "Diagnostic evaluation of a pleural effusion in adults: Initial testing" in UpToDate, F. Maldonado, Ed. (Wolters Kluwer, 2022).
32. F. Paul, S. K. D. Dellaripa, "Pulmonary manifestations of systemic lupus erythematosus in adults" in UpToDate, D. S. Pisetsky, Ed. (Wolters Kluwer, 2022).
33. A. Silva-Sanchez, T. D. Randall, Role of iBALT in respiratory immunity. Curr. Top. Microbiol. Immunol. 426, 21–43 (2019).
34. L. Shmuel-Galia et al., Dysbiosis exacerbates colitis by promoting ubiquitination and accumulation of the innate immune adaptor STING in myeloid cells. Immunity 54, 1137–1153.e8 (2021).
35. Y. J. Crow, D. B. Stetson, The type I interferonopathies: 10 years on. Nat. Rev. Immunol. 20, 1–13 (2021).
36. M. P. Rodero, Y. J. Crow, Type I interferon-mediated monogenic autoinflammation: The type I interferonopathies, a conceptual overview. J. Exp. Med. 213, 2527–2538 (2016).
37. A. Lepelley et al., Mutations in COPA lead to abnormal trafficking of STING to the Golgi and interferon signaling. J. Exp. Med. 217, e20200600 (2020).
38. O. Demaria et al., STING activation of tumor endothelial cells initiates spontaneous and therapeutic antitumor immunity. Proc. Natl. Acad. Sci. U.S.A. 112, 15408–15413 (2015).
39. H. Yang et al., STING activation reprograms tumor vasculatures and synergizes with VEGFR2 blockade. J. Clin. Invest. 129, 4350–4364 (2019).
40. J. D. Domizio et al., The cGAS-STING pathway drives type I IFN immunopathology in COVID-19. Nature 603, 145–151 (2022).
41. C. M. Card, S. S. Yu, M. A. Swartz, Emerging roles of lymphatic endothelium in regulating adaptive immunity. J. Clin. Invest. 124, 943–952 (2014).
42. R. Nadafi et al., Lymph node stromal cells generate antigen-specific regulatory T cells and control autoreactive T and B cell responses. Cell Rep. 30, 4110–4123.e4 (2020).
43. E. Vokali et al., Lymphatic endothelial cells prime naïve CD8+ T cells into memory cells under steady-state conditions. Nat. Commun. 11, 538 (2020).
44. X. Zhang et al., Discovery and mechanistic study of a novel human-stimulator-of-interferon-genes agonist. ACS Infect. Dis. 5, 1139–1149 (2019).
45. M. Li et al., Pharmacological activation of STING blocks SARS-CoV-2 infection. Sci. Immunol. 6, eabi9007 (2021).
46. F. Humphries et al., A diamidobenzimidazole STING agonist protects against SARS-CoV-2 infection. Sci. Immunol. 6, eabi9002 (2021).
47. D. Daoussis et al., A multicenter, open-label, comparative study of B-cell depletion therapy with Rituximab for systemic sclerosis-associated interstitial lung disease. Semin. Arthritis Rheum. 46, 625–631 (2017).
48. J. Munoz et al., Stimulator of interferon genes-associated vasculopathy with onset in infancy: A mimic of childhood granulomatosis with polyangiitis. JAMA Dermatol. 151, 872–877 (2015).
49. C. G. L. Raffaele et al., A patient with stimulator of interferon genes-associated vasculopathy with onset in infancy without skin vasculopathy. Rheumatology (Oxford) 59, 905–907 (2020).
50. K. C. Herold et al.; Type 1 Diabetes TrialNet Study Group, An anti-CD3 antibody, teplizumab, in relatives at risk for type 1 diabetes. N. Engl. J. Med. 381, 603–613 (2019).
51. A. A. Welcher et al., Blockade of Interferon-γ Normalizes Interferon-Regulated Gene Expression and Serum CXCL10 Levels in Patients with Systemic Lupus Erythematosus (Arthritis Rheumatol, Hoboken, NJ, 2015).
52. X. Hu, J. Li, M. Fu, X. Zhao, W. Wang, The JAK/STAT signaling pathway: From bench to clinic. Signal Transduct. Target. Ther. 6, 402 (2021).
53. J. Pilewski, "Evaluation and treatment of acute lung transplant rejection" in UpToDate, R. R. Hachem, Ed. (Wolters Kluwer, 2022).
54. G. A. Kolumam, S. Thomas, L. J. Thompson, J. Sprent, K. Murali-Krishna, Type I interferons act directly on CD8 T cells to allow clonal expansion and memory formation in response to viral infection. J. Exp. Med. 202, 637–650 (2005).
55. H. Ishikawa, G. N. Barber, STING is an endoplasmic reticulum adaptor that facilitates innate immune signalling. Nature 455, 674–678 (2008).
56. P. Bankhead et al., QuPath: Open source software for digital pathology image analysis. Sci. Rep. 7, 16878 (2017).
57. O. Yukselen, O. Turkyilmaz, A. R. Ozturk, M. Garber, A. Kucukural, DolphinNext: A distributed data processing platform for high throughput genomics. BMC Genomics 21, 310 (2020).
58. J. Reimand et al., Pathway enrichment analysis and visualization of omics data using g:Profiler, GSEA, Cytoscape and EnrichmentMap. Nat. Protoc. 14, 482–517 (2019).
59. P. Mande et al., Fas ligand promotes an inducible TLR-dependent model of cutaneous lupus-like inflammation. J. Clin. Invest. 128, 2966–2978 (2018).